Accepted manuscript doi:
10.1680/jmacr.22.00280

Accepted manuscript doi:
10.1680/jmacr.22.00280

Submitted: 28 September 2022

Published online in 'accepted manuscript' format: 24 February 2023

Manuscript title: Shear transfer in fly ash-concrete with electric arc furnace aggregates

Authors: Flora Faleschini[1,2], Daniel Trento[1], Vanesa-Ortega Lopez[3] and Mariano Angelo Zanini[1]

Affiliations: [1]Department of Civil, Environmental and Architectural Engineering, University of Padova, Padova, Italy; [2]Department of Industrial Engineering, University of Padova, Padova, Italy and [3]Department of Civil Engineering, Escuela Politécnica Superior, University of Burgos, Burgos, Spain

Corresponding author: Flora Faleschini, Department of Civil, Environmental and Architectural Engineering, University of Padova, Via Marzolo 9, 35131 Padova, Italy.

E-mail: flora.faleschini@dicea.unipd.it

Accepted manuscript doi:
10.1680/jmacr.22.00280

Abstract

This work experimentally evaluates the friction shear behavior of Electric Arc Furnace (EAF) concrete, compared to its reference counterpart made with natural aggregates only. For this scope, two concrete mixes were casted, both containing a blended cement with 30% of fly ash to improve their sustainability. For each mix, other than analyzing the main mechanical properties (compressive, tensile strength and elastic modulus), push-off specimens were tested to obtain the shear strength, failure modes, stress-slip and stress-crack opening curves. The results obtained here clearly identify an enhancement of the shear strength τ of EAF concrete compared to the reference, even though the relation between τ and concrete tensile strength f_{ct} is similar between the two concretes. Results are also compared with ones in literature, dealing with ordinary and recycled aggregate concrete (RAC). Further, existing models from both designing codes and literature were applied to the experimental results, obtaining conservative predictions in all cases. The safety margin for the EAF concrete was found to be higher than for the reference concrete.

Keywords: EAF concrete; mechanical properties; push-off; recycled concrete; shear strength

Accepted manuscript doi:
10.1680/jmacr.22.00280

1. INTRODUCTION

Shear failure is considered among the most dangerous failure types in reinforced concrete (RC) structures, because it occurs suddenly, without warning cracks, being thus a brittle phenomenon. For this reason, shear transfer mechanisms have been studied widely in literature, to evaluate mainly how concrete properties and steel arrangement influence shear transfer along a sliding plane. Among the different effects that play a role in the shear strength of RC members, aggregates interlock is worth to be mentioned: according to the first models by Walraven (1981) and Paulay and Loeber (1974), this phenomenon develops when the aggregates placed at one side of the crack come into contact with the cementing matrix of the other side, giving rise to tangential frictional stresses. Thus, aggregates interlock depends significantly on the crack opening, slip, and at a more in-depth level, on the aggregates' morphology, i.e. roughness, shape and size (Ruiz et al., 2015). In this context, the work by Sagaseta and Vollum (2011) is noteworthy, where the authors identified that even the mineralogic composition of the aggregate impacts on the shear strength transfer along cracks, experimentally observing differences among limestone and marine dredged gravel. They recorded a different brittleness between the aggregates, which affects cracks path, but lastly leads to achieve similar aggregates dilatancy values. Further, the strength of the cementitious matrix positively influences the shear strength (Fenwick and Paulay, 1968), as well as the presence of a confining pressure (Hobbs, 1974).

There are several experimental methods to investigate directly shear strength, but the most well-known is through push-off specimens (Mattock and Hawkins, 1972). Figure 1 provides a brief illustration of the test layouts that can be used to investigate shear transfer mechanisms on: a) Z-type push-off specimens (Soetens and Matthys, 2017); b) single-notched FIP-type specimens (FIP, 1978); c) double-notched push-through specimens, or modified JCSE SF6 specimens (Cuenca et al., 2020). Recall that some variations may exist, depending on the specific problem to be analyzed, e.g. the possible pre-cracking, steel reinforcement arrangement, specimen dimension, presence of confinement, etc. Particularly, the push-off test method (Figure 1a) allows to apply shear stresses along a prescribed sliding plane, which is identified through cut or casted notches in the specimen and ensures typically the most representative results, even if it is more difficult to be executed than the other layouts. The specimen is made with two L-blocks, connected together by a transverse element in the middle of the sample; the load is applied on the top surface, resulting in a direct shear along

Accepted manuscript doi:
10.1680/jmacr.22.00280

the plane that connects the two edges of the notches (colored in red, in Figure 1a). The main advantage of adopting such test method is that the specimens have small dimensions, and that the shear sliding plane can be easily identified: in this manner, it is possible to carry out many experimental tests, to address the specific influence of the analyzed variable, which is clearly difficult to manage when real-scale elements are tested. Additionally, when testing RC beams failing in shear, the interaction with bending actions is clearly not negligible.

In this context, the development of new, sustainable concretes, where the natural aggregates are replaced with recycled ones, opens the question about how this substitution influences the shear strength of the RC elements, and mainly, how it impacts on the aggregates interlock shear transfer mechanism. Several works attempt to provide a solution to this query, depending on the addition provided in the mix, or on the recycled material that substituted the natural aggregate. In the first group of concretes, it is worth mentioning the works carried out on fiber reinforced concrete (FRC), where the addition of dispersed fibers in the matrix allows to carry a significant portion of the shear stresses (Minelli and Plizzari, 2013; Barr, 1987). Experimental results carried out on push-off (Barragan et al, 2006) and modified push-off specimens (Echegaray-Oviedo et al., 2017) demonstrate clearly the crack bridging ability of steel fibers, when subject to a combination of both mode I (opening) and mode II (sliding) crack propagation, confirmed by the same evidences obtained on modified JCSE SF6 specimens (Soetens and Matthys, 2017).

A series of research carried out to study the influence of recycled materials introduction on concrete shear strength belong to the second group of works: however, only few of them were carried out under pure shear failure. Fonteboa et al. (2010) investigated the shear strength of recycled aggregate concrete (RAC), observing a reduction of shear friction capacity, especially when specimens are designed without transverse reinforcement. Xiao et al. (2012) obtained the same results, and identified the cause of such strength loss into the presence of microcracks and internal damage of the attached mortar of the recycled aggregate (RA). Fakitsas et al. (2012) confirmed these observations, showing that the shear planes in high-strength concrete with RA go through the aggregates, rather than around it, thus reducing the shear strength value. Instead, in normal strength concrete Rahal and Hassan (2021) demonstrated that the failure surfaces in RAC were generally less rough than in natural aggregate concrete (NAC), due to the development of the cracks along the old ITZ of the RA, being weaker than the new cementitious matrix. However, when confined, the shear strength

Accepted manuscript doi:
10.1680/jmacr.22.00280

improves substantially, as numerically validated also in (Sun et al., 2018). This result is due to the effect of the compression force applied normally to the interface, that increases the contribution of aggregate interlock and friction, in the same way in RAC than in NAC. Waseem and Singh (2016) studied instead the shear stress-slip relationships of RAC compared to NAC in push-off specimens, both transversally reinforced with stirrups and without. When the reinforcement is present and it crosses the shear interface, clamping and dowel actions affect significantly the shear strength development. They also applied some existing models for strength prediction, with sufficient good results. Trindade et al. (2020) and Rahal and Al-Khaleefi (2015) obtained a conservative prediction of the shear strength when using ACI code (2019), even if the shear strength of RAC is inferior to that of NAC; however, unconservative predictions are obtained with other formulations. More recent works attempt to study the interaction with RAC with steel fibers (Gao et al., 2017), and the direct shear strength of other concrete types, e.g. with alkali-activated slag (Manjunath et al., 2020).

According to the knowledge of the authors, no specific studies were carried out, until now, to understand shear transfer in Electric Arc Furnace (EAF) concrete. This kind of sustainable concrete is realized substituting natural aggregates with EAF slag, which is a very hard, black, stony-like, recycled material, coming from steelmaking industry (Figure 2). Several works in literature demonstrated that EAF concrete demonstrates similar, and even superior, mechanical properties than NAC (Monosi et al., 2016; Abu-Eishah et al., 2012; Arribas et al., 2015), especially when EAF slag is used in the coarse grading fraction (Faleschini et al., 2015). Promising results were obtained about the adoption of this concrete for structural applications, as observed testing different real-scale elements, both RC beams under flexure-shear (Faleschini and Pellegrino, 2013; Santamaria et al., 2021), RC columns under axial loading (Lee et al., 2018), RC beam-column joints under cyclic reversed lateral loading with flexural-shear failure (Faleschini et al., 2017a). Some recent results highlighted that, both under gravity loads (Zanini, 2019) and seismic solicitation (Faleschini et al., 2019), the use of EAF concrete allows attaining the same, or even higher, structural reliability than NAC. However, for a proper interpretation of the shear capacity of this kind of concrete, and its further safe use in RC structures, an experimental program aimed at assessing the aggregates interlock and friction contribution to shear strength is required, which is the topic covered by this work. Here some results are shown for the specific case of a sustainable EAF concrete mix, designed with 100% of coarse EAF aggregates replacing the natural gravel and with a

blended cement with 30% of fly ash. Specifically, plain un-notched push-off specimens were tested, without transverse reinforcement, in order to compare the results with literature ones obtained from specimens with similar geometry and steel reinforcement details, but made with RAC. Additionally, the suitability of some current formulations from literature and existing Codes is evaluated, both to predict the basic mechanical EAF concrete properties, and both to evaluate its shear strength. Results will allow to evaluate if the same accuracy can be obtained when using such formulations, originally developed only for NAC mixes.

2. EXPERIMENTAL PROGRAM

2.1 Materials and mix design

Two concrete mixes were designed: NAC and EAF concrete. The former contains natural aggregates only, whereas in the latter EAF slag substitutes the natural gravel. The aggregates fine fraction (0-4 mm) is the same for both the mixes, and it is made with river sand. The physical properties of aggregates are listed in Table 1, whereas Figure 3 shows the aggregates grading curves: note that three fractions of EAF slag are used to replace the 4-16 mm NA fraction, in different proportions. All the mixes were realized adopting a cement CEM IV/A (V) 42.5 R, according to (UNI EN 197-1, 2011): the choice of adopting a pozzolanic cement, with about 30% of fly ashes replacing clinker, allows to achieve a more sustainable mix, with a lower carbon footprint than a concrete made with Portland cement, which however is characterized by a rapid-strength gain. A similar cement type (CEM IV/B), which contains much larger quantities of supplementary cementing materials (SCM), was already used by Santamaria et al. (2020) in combination with EAF slag: in that case, the experience of the authors was not positive, since undesirable thixotropic phenomena occurred both in pumpable and self-compacting mixes, leading to a non-satisfactorily combination of the two materials. Here, an attempt to adopt synergistically the two materials is made, assuming that less SCM in the blended cement will not affect the workability of the mix. Lastly, to cast the concrete mixes, tap water from the city of Padova, Italy, is used, which does not contain any harmful substances, and a super-plasticizing sulphonated naphthalene admixture is added at different percentages on cement weight to reach the required consistency.

Table 2 shows the mix design of the two concretes. For each of them, the following specimens were casted: two cylinders per each property, with d x h = 100 x 200 mm, to evaluate compressive strength (f_c) at 14, 28 and 56 days, indirect tensile strength (f_{ct}) and elastic modulus (E_c) at 28 days; three push-off samples. The number of samples was limited

due to a reduced capacity of the mixer. After concrete casting, all the samples were covered by humid tissues and sealed in plastic bags until demolding after 24 hours; then, they were cured in water at 20±1°C until the time of testing.

2.2 Push-off specimens and test setup

To study the shear transfer mechanism in EAF concrete, the push-off test method was adopted, which specimens' geometry is shown in Figure 4. The geometry is similar to that used in (Rahal and Al-Khaleefi, 2015; Mathews et al., 2021). The height of each specimen was 260 mm, having a rectangular cross-section of b x h = 140 x 100 mm. The specimens have two intermediate notches, directly realized thanks to the shape of the formwork, which allow to control the flow of the stresses and aim to concentrate the development of shear stresses properly across the plane of contact between the two halves of each specimen. This region of the specimen is the shear-transfer plane, where both shear and normal stresses act simultaneously. Four deformed L-shaped longitudinal bars with 10 mm diameter were located in the specimens to prevent possible flexural failure outside the investigated shear-plane region, which are supported by six transverse bars with 6 mm diameter. Steel type was B450C for both the reinforcement diameter bars, according to (NTC, 2018). Their main mechanical properties are shown in Table 3, which lists the tensile yielding f_y and ultimate f_t strength values, at the corresponding yielding ε_y and ultimate ε_t strain. No transverse reinforcement is present crossing the shear plane, similarly than in (Fonteboa et al., 2010) for the condition of $\rho_v = A_{sw}/A_c = 0\%$, where A_{sw} is the transverse steel area, A_c is the concrete area in the sliding plane, and ρ_v is the volumetric transverse reinforcement ratio. The same configuration was used in (Barragan et al., 2006; Waseem and Singh, 2016; Raha and Al-Khaleefi, 2015; Mathews et al., 2021). In this way, the pure effect of friction contribution to the shear strength can be analyzed, without focusing, at this stage, to the interaction with the reinforcement. In fact, it is worth recalling that non-ordinary concretes, e.g. made using recycled or lightweight aggregates, or high-strength concretes, are subject to different aggregate interlock mechanisms due to different crack kinematics (Fang et al., 2020, Ruiz 2021).

The specimen is loaded in a universal 600 kN capacity machine, through a monotonically loading under displacement control, fixed at 0.3 mm/min, similarly than in (Yusuf et al., 2019). Figure 5 shows one push-off specimen before loading, where it is possible to observe the testing instrumentation: four linear voltage displacement transducers (LVDT) and two

Accepted manuscript doi:
10.1680/jmacr.22.00280

displacement and strain transducers (DST) were used. Particularly, two pairs of LVDT were used per each face of the specimen: the displacement recorded by each instrument (D_1 and D_2) is used to calculate the relative vertical slip (s) between the two L-halves, according to Eq. 1:

$$s_i = D_{1,i} - D_{2,i} \quad (1)$$

for each i-face of the specimen. The precision of the LVDT is ± 0.01 mm, over a gage length of 20 mm. Instead, the DST provides directly the crack opening in the transverse direction, because they are placed crossing the shear plane, similarly than in (da Cunha et al., 2022). Their precision is ± 0.001 mm, with a maximum opening of 2.5 mm. Note also that in the loading machine a hinge connection is present on the top of the actuator: this solution aims to maintain the applied load as much axial as possible, thus minimizing bending solicitations emerging from the irregularities possibly present in the specimens, and maintaining a pure shear action in the analyzed region of the specimen. With the same objective, a restraining steel plate and a thin layer of high-strength mortar are placed on both the top and bottom of the specimens, to minimize the effect of some discontinuities and irregularities on those surfaces.

3. RESULTS

In this section, the results of the experimental campaign are discussed, in terms of: fresh behavior and mechanical properties at 14, 28 and 56 days; shear strength and failure mode of push-off specimens; shear stress vs. slip curves; shear stress vs. crack opening curves.

3.1 Fresh behavior and concrete mechanical properties

Table 4 lists the results obtained in terms of average fresh density ρ_c, Abram's cone slump, hardened density $\rho_{c,28}$, compressive strength f_c at 14, 28 and 56 days, indirect tensile strength through splitting test f_{ct} and secant Elastic modulus E_c at 28 days.

According to Santamaría et al. (2020), when pozzolanic cement with large amounts of SCM is used, a significant reduction of workability is experienced, so large that Santamaria et al. (2020) suggested that the combination between CEM IV/B and EAF slag is probably hindered. Here, instead, the workability of the EAF concrete with CEM IV/A, which differs from CEM IV/B by the amount of SCM, is maintained sufficiently good, and the fresh concrete has the same slump class than the NAC mix, which is a S3 consistency class, defined according to (UNI EN 206-1, 2014). Only a few reductions of slump value compared to NAC was exhibited, due to well-known shape effect of the EAF slag, which makes the

fresh EAF concrete more difficult to be placed and worked (Santamaría et al., 2017). Typically, an adjustment of the fine particles content in the mix is sufficient to prevent this phenomenon. Further, during casting operations, no sudden workability loss was experienced, thus proving the feasibility of combining slag aggregates with pozzolanic cement, at least from a workability point of view.

Concerning mechanical properties, the results obtained here confirm the current knowledge about EAF concrete: indeed, the EAF mix exhibits compressive strength increases of about + 44%, + 37% and + 34% for the 14, 28 and 56 curing days, compared to the NAC. The same applies for the tensile strength, with + 28%, and the Elastic modulus, with + 36%. These results confirm also the good interaction of the slag with the blended cement, which allows even a more rapid strength gain than in NAC, and a continuous later strength development, as observed from the results of 56 days curing time. Strength enhancement, compared to NAC, has been already explained in literature, as a consequence of some concurrent causes: intrinsic greater strength of EAF aggregates than NA, linked to the high content of iron oxides (Roslan, 2020); high adhesion between the slag and cementitious matrix, due to the EAF slag shape effect (Tamayo et al., 2019); high quality of the interfacial transition zone (ITZ), due to enrichment, in the aggregate wall zone, of the products from the late hydration of the slag itself (Arribas et al, 2015).

3.2 Assessment of mechanical properties based on Codes prediction

Table 5 shows the comparison between the experimental and predicted values of concrete tensile strength and elastic modulus, based on the formulations of ACI 318 (2019) and Eurocode 2 EC2 (2004). It is worth recalling that very often only compressive strength is experimentally investigated to characterize a concrete mix, as a quality control measure, whereas the other mechanical properties are only seldom tested in the practice. Concerning f_{ct}, it is often expressed as a power of the compressive strength. According to ACI 318 (2019) and EC2 (2004), the average tensile strength f_{ctm} (at 28 days) can be estimated respectively as:

$$f_{ctm} = 0.56 \cdot \sqrt{f_{cm}} \qquad (2)$$

$$f_{ctm} = \begin{cases} 0.3 \cdot {f_{ck}}^{2/3}, f_{ck} < 50 \\ 2.12 \cdot ln \cdot (1 + 0.1 \cdot f_{cm}), f_{ck} \geq 50 \end{cases} \qquad (3)$$

where f_{ck} and f_{cm} are the characteristic and average compressive strength at 28 days, which are linked, in a simplified approach, by the following relation:

$$f_{ck} = f_{cm} - 8MPa \qquad (4)$$

The estimated f_{ctm} with Eqs. 2-3 differ respectively from the experimental values by 2 and 17% for the NAC, whereas by 11 and 17% for the EAF. Both the equations underestimate the f_{ctm} values, regardless of the mix; the prediction of ACI 318 is more accurate than that of EC2. However, the error made by the EC2 formulation is constant for the two mixes, whereas that made by ACI 318 changes highly, being almost precise for the NAC and much less for the EAF mix. This result is due to the fact that these formulations were both calibrated on ordinary concretes, and the EC2 uses the characteristic value instead of the average for the compressive strength, thus being implicitly more conservative.

The average elastic modulus E_{cm} (at 28 days) can be estimated again as a power function of the compressive strength, according to ACI 318 (2019) and EC2 (2004), respectively:

$$E_{cm} = 4700 \cdot \sqrt{f_{cm}} \qquad (5)$$

$$E_{cm} = 22000 \cdot \left(\frac{f_{cm}}{10}\right)^{0.3} \qquad (6)$$

Eqs. 5 and 6 both overestimate the E_{cm} value for the NAC mix of +4% and +17%, whereas they underestimate it for the EAF concrete of -10% and -5%, respectively. It is worth to note that EC2 formulation allows for a correction of the predicted value that depends on the aggregates type, and that can be considered as a density-correction factor. Particularly, for basalt aggregates the value of E_{cm} should be increased by 20%; in case of lightweight aggregates a reduction ranging between 10 and 20% is applied. Other works demonstrated that the inclusion of such modification improves the estimation of the E_{cm} value compared to other Codes, especially for those concreted with light-weight or heavy-weight aggregates (Revilla-Cuesta et al., 2022). In this case, applying a correction of +5% for the EAF aggregates, the prediction has a very high accuracy, with an error of less than 1%.

3.3 Shear transfer test: main results

The main test results of the experimental campaign are listed in Table 6, which collects the following information: the ultimate load P_u (kN); the ultimate shear strength τ_u (MPa), evaluated as P_u/A_c, where A_c is the shear plane area (here, 9000 mm^2); the average ultimate slip, evaluated at P_u; and the average ultimate crack width w_u, evaluated at P_u. Results are shown for each of the tested specimens, and then average (*ave.*) and standard deviation (*st.dev.*) values are also presented.

Accepted manuscript doi:
10.1680/jmacr.22.00280

3.3.1 Shear strength and failure modes

EAF concrete displays higher shear strength values than NAC, with an average enhancement of +30%. Results are characterized by almost the same scatter, as proved by the similar *st.dev.* value, and by the same coefficient of variation *COV* = *st.dev./ave.* = 0.10, in both the cases. This result represents a fundamental point for ensuring a widespread use of EAF concrete for structural applications, because it means that the heterogeneity possibly present in a recycled material does not affect substantially the homogeneity of concrete properties.

Shear strength values are then divided by $f_c^{1/2}$ and by f_{ct}, to obtain the following parameters, respectively: τ_u^* and τ_u^+. Indeed, several works reported a clear effect of concrete mechanical properties on the shear strength, typically dependent on $f_c^{1/2}$ (Rahal et al., 2016), which is a simplified way to define f_{ct}, as seen above according to ACI 318 (2019). As recalled in Section 3.2, however, when dealing with non-conventional concretes, the relation between f_c and f_{ct} might not follow the same laws for NAC: in fact, the accuracy of the prediction of f_{ct} depending on $f_{cm}^{0.5}$ (with Eq. 2) changes significantly between NAC and EAF mixes. This result depends on the EAF slag interaction with the cementitious matrix, that properly modifies the interface characteristics, the thickness of the ITZ and the adhesion strength. Such evidence was also discussed in (Faleschini et al., 2017b), when dealing with bond of EAF concrete with steel rebars. Table 7 lists the dimensionless τ_u^* and τ_u^+ values: it is possible to observe again that both τ_u^* and τ_u^+ are higher in EAF concrete than in NAC. However, the average increase in τ_u^* observed for the EAF specimens is about + 10% only: such result reveals that the enhanced mechanical properties due to EAF slag substitution in place of NA contribute substantially for the shear strength enhancement. The increase in τ_u^+ for the EAF concrete compared to the NAC is instead marginal (1% only): the mixes have practically the same dimensionless τ_u^+ value, which indicates that splitting tensile strength can be well correlated with the shear strength, at least in this case. Thus, the enhancement of EAF concrete shear strength may be attributed, other than to the increased strength of the slag, to the aggregates sharp shape, affecting also the concrete tensile behavior, which allows contact areas to be developed and to increase the friction between the two L-blocks, consistently with (Yang et al., 2017).

Accepted manuscript doi:
10.1680/jmacr.22.00280

Concerning the failure modes, Figure 6 shows two representative specimens, one for NAC (a) and one for EAF (b) concrete, after the test. When loaded, the specimens did not display any visible cracking phenomena until more the 90% of the peak load; only when approaching the maximum applied load, some cracks started open. The failure occurred in a brittle way, with the sudden formation of a first thick tension vertical and then sub-vertical cracks, crossing the shear plane and identifying a compressed strut. The first crack, which is the thickest one, appears first at one notch edge and it is typically vertical; ones the pattern achieves the second notch edge, then the second main sub-vertical crack grows rapidly until failure. These cracks were inclined at maximum 30° from the shear plane. The failure mode is dominated by tensile splitting. The absence of any transverse reinforcement crossing the shear plane did not allow to maintain a certain load after the peak, resulting in a definitive separation between the two L-blocks that constitute the push-off specimen. The same applies for the slip: initially, no clear slip was evident; instead, the observed movement can be linked more to a relative rotation between the two blocks due to the compression of the inclined concrete strut that formed. For sake of brevity, in this paper, we will refer to this displacement as slip, too. Then, a sudden increase of the slip occurs, resulting in an extensive separation of the two L-blocks.

Figure 7 shows the split surface of NAC (a) and EAF (b) concrete, after testing. In both the figures, it is possible to distinguish two phenomena (see Figure 8) when an aggregate is present in the shear surface: first, the cracks may pass directly through the aggregates, which are thus cut in two separate portions; second, cracks may propagate around the aggregates, concentrating in the ITZ. Both phenomena are present in NAC and EAF specimens, with a main difference: in EAF, aggregates failure dominate; in NAC, the two cracking paths occur almost with the same frequency. This behavior is also confirmed when looking at the splitting surfaces obtained after indirect tensile strength tests of NAC and EAF concrete. When analyzing crack paths, one should recall that: failure in EAF occurred at a load about +29% higher than in NAC; the cementitious matrix has a relatively good quality, as the cement dosage is quite high. Thus, it is possible to state that the good ITZ quality of the EAF concrete allowed to postpone one type of failure, but when the shear stress exceeds a certain limit, the specimens failed due to aggregates cracking, as it happens in high strength concretes (Figure 8b). Thus, the bond strength between the matrix and the slag should be similar or even higher than the tensile strength of the EAF aggregate particles. Both bond and

Accepted manuscript doi:
10.1680/jmacr.22.00280

tensile strengths in EAF concrete are higher than the respective values in NAC. Furthermore, the crack surface exhibits significant angularities and roughness that allow a certain contact area to develop.

3.3.2 Shear stress vs. slip curves

Shear stress vs. slip curves are plotted in Figure 9, obtained as the average from the four LVDTs used for each specimen. The curves are plotted until reaching the ultimate shear strength value, then they are interrupted due to the occurrence of the brittle failure of the specimens. The maximum shear strength cannot be maintained after the peak, thus the curves display a sudden decrease which is not plotted here because of the few sense of slip records. From these curves, the values of s_u listed in Table 5 are obtained: EAF concrete is characterized by less slip values, in average -26 % than NAC. The *COV* value is instead similar between the two concrete types, being 0.26 for NAC and 0.22 for EAF concrete. According to these results, it is possible to state that the behavior of EAF concrete is more brittle than NAC: indeed, as the strength increase, the brittleness of concrete increases as well (Hamadi and Reagan, 1980). This result is confirmed also looking at the slope of the curves in Figure 9, which define the shear stiffness, higher for EAF than NAC concrete. However, in general, the deformative behavior of the two types of concretes is similar.

3.3.3 Shear stress vs. crack opening curves

Shear stress vs. crack opening curves are plotted in Figure 10, obtained as the average from the two DSTs used on the two faces of each specimen. For specimen EAF_2, it was not possible to provide the whole curve, because the cracks let the instrumentation to detach. All the other curves are plotted until reaching the ultimate shear strength value, similarly for the stress vs. slip ones. The values of w_u listed in Table 5 are obtained from the curves in Figure 10, at shear stress peak: NAC and EAF concrete have almost the same ultimate crack width in average, with a variation between them of only 2%. Such ultimate crack width value is considerably low, being in all cases less than 0.1 mm, consistent with the brittle failure mode. Further, for both the concrete mixes, the scatter of the results is similar and higher compared to all the other analyzed properties. Indeed, the *COV* value is more than 35% for both NAC and EAF concrete.

Accepted manuscript doi:
10.1680/jmacr.22.00280

4. DISCUSSION

4.1 Comparison with literature results on NAC and RAC

Few works in literature analyzed the shear transfer in concretes with recycled constituents by means of push-off specimens, and only some of them used specimens without any transverse reinforcement. Fonteboa et al. (2010) studied shear friction capacity of concretes containing recycled concrete aggregates (RCA) and silica fume addictions in push-off specimens with ρ_v ranging between 0 and 0.57%. They tested four mixtures with nominal cement dosage 325 kg/m^3 and w/c=0.55, and specimens are labelled as it follows: NAC, RAC, NACS and RACS. The nomenclature identifies, respectively, a conventional NAC, a mix with 50% of RCA and other two NAC and RAC which differ per the addiction of silica fume only. Waseem and Singh (2016) evaluated the shear transfer in normal and high strength RAC. In order to analyze the contribution of the stirrups, they used different percentages of ρ_v. They casted three mixtures of normal concrete (nominal cement dosage 435 kg/m^3 and w/c=0.45) with RCA replacement percentage ranging from 0 to 100 % of the total coarse aggregate fraction, named as N00, N50 and N100, respectively. Other three mixtures are high strength concretes (nominal cement dosage 546 kg/m^3 and w/c=0.28) with the same proportion on the coarse aggregate fraction, named as H00, H50 and H100 respectively. A recent research work by Yusuf et al. (2019) analyzed the shear transfer mechanisms in non-transversally reinforced NAC and RAC specimens, before and after high temperature exposure. They casted similar concrete mix designs than the ones of the present experimental campaign, i.e., with cement dosage of 416 kg/m^3 and w/c = 0.52, and with little amount of superplasticizer. The authors substituted the crushed limestone used as natural aggregate with increasing percentage of RA, this being 0 – 30 – 70 – 100%, and labelled them as NAC, RAC30, RAC70 and RAC100, respectively. Since the mixtures casted by Yusuf et al. (2019) are similar to the ones of this work in terms of mechanical strength at room temperature, the experimental results are well comparable to the ones obtained in the present research. Note that, compared to the NAC tested here, Yusuf et al. (2019) adopted crushed aggregates, both natural and recycled, which in general ensure good friction mechanism development during shear sliding, because of the high contact areas between the particles and matrix. Figure 11 shows a comparison of the average normalized (to both $fc^{0.5}$ and f_{ct}) shear strength from this work and the others from literature.

Accepted manuscript doi:
10.1680/jmacr.22.00280

Overall, the results obtained in this work agree with those of NAC and RAC having similar mix design and strength, with EAF concrete displaying even higher shear strength than most of the RAC counterparts. Only the results from Fonteboa et al. (2010) are characterized by higher normalized shear strength, because of the addiction of silica fume, which was found to balance the loss of shear strength typically observed in RAC, thanks to the improvement of the cement matrix and thus of the ITZ quality. The use of recycled aggregates is almost always detrimental for the shear strength development and also for other mechanical properties (Fakitsas et al., 2012), because of the lower strength of RA than NA (Silva et al., 2015). This is exactly the opposite of what happens in concretes casted replacing NAs with EAF slag: indeed, the replacement is made with an aggregate characterized, generally, by a remarkable higher strength than the ordinary gravel. Despite at failure the cracks passed mainly through the EAF aggregates, as opposite than in NAC specimens, where they passed both through NAs and around them, the shear transfer capacity is higher in EAF concrete, thanks also to a sort of interlocking at the macro-level, similarly to what obtained by Sagaseta and Vollum (2011) and Haskett et al. (2011). Such phenomenon occurs thanks to the irregular shape of the crack surfaces, which allows contact areas to develop, despite the aggregate particles fracture almost completely at cracks (see the comparison between Figure 7a and 7b).

4.2 Existing shear friction formulations

There are several codes and literature formulations that can be used to provide the shear transfer strength, developed mainly for the verifications of concrete construction joints. Most of them are based on Coulomb failure criterion, because as the shear stress increases across an interface, most of the load is carried by the concrete-to-concrete cohesiveness:

$$\tau = c + \mu \cdot \sigma_{ncr} \qquad (7)$$

where, other than the shear stress τ, c is the cohesion (typically, a percentage of the splitting tensile strength), μ is the coefficient of friction along the shear plane (depending on the roughness of the interface), σ_{ncr} is the normal stress to the shear plane, that is connected to the amount of confinement provided by the transverse reinforcement crossing the shear plane. When adopting such formulation type for the case analyzed in this work, the second term of the addition goes to zero, because of the absence of transverse reinforcement. Thus, τ is constant and it can be estimated according to the proposal of the single code/author, just depending on the crack surface roughness. Note that all the formulations based on Eq.7 were developed primarily for ordinary concretes, where cracks do not cross directly the aggregates

Accepted manuscript doi:
10.1680/jmacr.22.00280

but propagate around them. Only in some cases, some authors were more specific and proposed particular value for different aggregate types (Loov and Patnaik, 1994; Climaco and Regan, 2001). Table 8 lists some common expressions and values for estimating the shear strength under the testing condition of this work, thus providing the estimation of the experimental τ: it is possible to see that the predictions are quite rough, and generally underestimate by more than half the experimental values. In Table 8, the predictions that contain f_{ctk}, i.e., the characteristic tensile strength, and f_{ctd}, i.e. the design tensile strength, are simplified here through the average tensile strength, thus any partial safety factor was not applied. Even with such simplification, the predictions are far from the observed values, with a maximum $\Delta = \tau_{u,th} / \tau_{u,exp}$ value of 0.682, provided by Hamadi and Regan (1980) model for gravel aggregates. The results are more conservative for EAF concretes than for NAC, thus the safety margin is even higher for EAF than the ordinary concrete, despite of the different cracking path at the interface between the two concretes.

5. CONCLUSIONS

In this work, the effects of adopting a different type of recycled coarse aggregate, namely the Electric Arc Furnace slag, on the mechanical properties and shear strength of plain concrete are experimentally analyzed. Specifically, concerning shear transfer mechanisms, push-off specimens were tested. One element of novelty analyzed here is the synergistic adoption of a blended cement with fly ash together with EAF slag, that allowed to cast a workable mix with good mechanical performances. The main conclusions that were achieved from this work on the shear strength of EAF concrete, about which no other experimental evidence in literature was found until now, can be summarized as it follows:

- EAF concrete displays higher shear strength than NAC, as observed from push-off tests without transverse reinforcement or confining solicitations. All specimens show brittle failure when the maximum load was reached. There is no difference in the global failure mode between NAC and EAF concrete, even if the exhibited crack path along the interface differs;
- It is possible to distinguish two phenomena when an aggregate is present in the shear surface: in EAF concrete, at this cement dosage and w/c content, aggregates failure dominates; in NAC, cracks mostly cross the aggregates or propagate around them. However, the crack surface in the EAF concrete are highly rough and present many

angularities, thus allowing for the development of several contact areas, increasing the shear strength thanks to a macro-scale aggregate interlock;

- Existing shear friction formulations based on Mohr-Coulomb approach, developed for ordinary concretes with NA, are very conservative for the analyzed case, where only the cohesiveness parameter is accounted for. The formulations predict better the experimental values for NAC than for EAF concrete. However, the safety margin for the EAF concrete is higher than for NAC.

Acknowledgements

The authors would like to express their acknowledgement to Zerocento S.r.l. for providing the EAF slag.

Notation

s the relative vertical slip
ρ_c average fresh density
f_c compressive strength
E_c Elastic modulus
f_{ctm} the average tensile strength
f_{ck} and f_{cm} are the characteristic and average compressive strength at 28 days
E_{cm} the average elastic modulus
P_u the ultimate load (kN)
τ_u the ultimate shear strength (MPa)
A_c is the shear plane area
w_u the average ultimate crack width
τ the shear stress
c is the cohesion
μ is the coefficient of friction
σ_{ncr} is the normal stress to the shear plane

References

Abu-Eishah, S. I., El-Dieb, A. S., & Bedir, M. S. (2012). Performance of concrete mixtures made with electric arc furnace (EAF) steel slag aggregate produced in the Arabian Gulf region. *Construction and Building Materials*, 34, 249-256.

ACI 318-19. (2019) Building Code Requirements for Structural Concrete and Commentary.

Arribas, I., Santamaria, A., Ruiz, E., Ortega-Lopez, V., & Manso, J. M. (2015). Electric arc furnace slag and its use in hydraulic concrete. *Construction and Building Materials*, 90, 68-79.

Barr, B. (1987). Fracture characteristics of FRC materials in shear. *ACI Special Publication*, 105, 27-54.

Barragan, B., Gettu, R., Agullo, L., & Zerbino, R. (2006). Shear failure of steel fiber-reinforced concrete based on push-off tests. *ACI Materials Journal*, 103(4), 251.

Climaco J. C. T. S. and Regan P. E. (2001). Evaluation of bond strength between old and new concrete in structural repairs. *Magazine of Concrete Research*, 53(6), 377-390.

Cuenca, E., Conforti, A., Monfardini, L., & Minelli, F. (2020). Shear transfer across a crack in ordinary and alkali activated concrete reinforced by different fibre types. *Materials and Structures*, 53(2), 1-15.

da Cunha, B. F., de Andrade Pinto, R. C. & Savaris, G. (2022). Evaluation of self-consolidating concrete shear strength by means of push-off test. *Magazine of Concrete Research*, 1-10.

Echegaray-Oviedo, J., Navarro-Gregori, J., Cuenca, E., & Serna, P. (2017). Modified push-off test for analysing the shear behaviour of concrete cracks. *Strain*, 53(6), e12239.

EN 1992-1-1 (2004). Eurocode 2: Design of concrete structures.

Faleschini, F., Fernández-Ruíz, M. A., Zanini, M. A., Brunelli, K., Pellegrino, C., & Hernández-Montes, E. (2015). High performance concrete with electric arc furnace slag as aggregate: Mechanical and durability properties. *Construction and Building Materials*, 101, 113-121.

Faleschini, F., Hofer, L., Zanini, M. A., dalla Benetta, M., & Pellegrino, C. (2017a). Experimental behavior of beam-column joints made with EAF concrete under cyclic loading. *Engineering Structures*, 139, 81-95.

Faleschini, F., & Pellegrino, C. (2013). Experimental behavior of reinforced concrete beams with electric arc furnace slag as recycled aggregate. *ACI Materials Journal*, 110, 197-206.

Faleschini, F., Santamaria, A., Zanini, M. A., San Jose, J. T., & Pellegrino, C. (2017b). Bond between steel reinforcement bars and Electric Arc Furnace slag concrete. *Materials and Structures*, 50(3), 1-13.

Faleschini, F., Zanini, M. A., & Toska, K. (2019). Seismic reliability assessment of code-conforming reinforced concrete buildings made with electric arc furnace slag aggregates. *Engineering Structures*, 195, 324-339.

Fang, Z., Jiang, H., Liu, A., Feng, J., & Li, Y. (2020). Shear-friction behaviour on smooth interface between high-strength and lightweight concrete. *Magazine of Concrete Research*, 72(2), 68-87.

Fakitsas, C. G., Papakonstantinou, P. E. A., Kiousis, P. D., & Savva, A. (2012). Effects of recycled concrete aggregates on the compressive and shear strength of high-strength self-consolidating concrete. *Journal of Materials in Civil Engineering, ASCE*, 24(4), 356-361.

Fenwick, R. C., & Paulay, T. (1968). Mechanisms of shear resistance of concrete beams. *Journal of the Structural Division, ASCE, 94*(10), 2325-2350.

Fonteboa, B. G., Martínez, F., Carro, D., & Eiras, J. (2010). Shear friction capacity of recycled concretes. *Materiales de Construcción*, 60(299), 53-67.

FIP - Federation Internationale de la Precontrainte. (1978). Shear at the interface of precast and in situ concrete. *FIP* shear test. *FIP*, Lausanne.

Gao, D., Zhang, L., & Nokken, M. (2017). Mechanical behavior of recycled coarse aggregate concrete reinforced with steel fibers under direct shear. *Cement and Concrete Composites*, 79, 1-8.

Hamadi, Y.D., & Reagan, P.E. (1980). Behavior of normal and lightweight aggregate beams with shear cracks. *The Structural Engineer* 58B(4): 71-79.

Haskett, M., Oehlers, D. J., Ali, M. S. M. & Sharma, S. K. (2011). Evaluating the shear-friction resistance across sliding planes in concrete. *Engineering Structures*, 33(4), 1357-1364.

Hobbs, D. W. (1974). Strength and deformation properties of plain concrete subject to combined stress. Part 3: Results obtained on a range of flint gravel aggregate concretes (No. 42.497 Tech. Rpt.).

Lee, J. M., Lee, Y. J., Jung, Y. J., Park, J. H., Lee, B. S., & Kim, K. H. (2018). Ductile capacity of reinforced concrete columns with electric arc furnace oxidizing slag aggregate. *Construction and Building Materials*, 162, 781-793.

Loov, R.E., & Patnaik, A.K. (1994). Horizontal shear strength of composite concrete beams with a rough interface. *PCI journal*, 39, 1.

Manjunath, R., Narasimhan, M. C., Shashanka, M., Vijayanand, S. D., & Vinayaka, J. (2020). Experimental studies on shear strength characteristics of alkali activated slag concrete mixes. *Materials Today: Proceedings*, 27, 275-279.

Mathews, M. E., Anand, N., Lublóy, É., & Kiran, T. (2021). Effect of elevated temperature on interfacial shear transfer capacity of self-compacting concrete. *Case Studies in Construction Materials*, 15, e00753.

Mattock, A. H., & Hawkins, N. M. (1972). Shear transfer in reinforced concrete - Recent research. *PCI Journal*, 17(2), 55-75.

Minelli, F., & Plizzari, G. A. (2013). On the Effectiveness of Steel Fibers as Shear Reinforcement. *ACI Structural Journal*, 110(3).

Monosi, S., Ruello, M. L., & Sani, D. (2016). Electric arc furnace slag as natural aggregate replacement in concrete production. *Cement and Concrete Composites*, 66, 66-72.

NTC 2018. (2018). Norme Tecniche per le Costruzioni – Ministerial Decree 18/01/2018. *In Italian.*

Paulay, T., & Loeber, P. J. (1974). Shear transfer by aggregate interlock. *ACI Special Publication*, 42, 1-16.

Rahal, K. N., & Al-Khaleefi, A. L. (2015). Shear-friction behavior of recycled and natural aggregate concrete-An experimental investigation. *ACI Structural Journal*, 112(6), 725.

Rahal, K. N., Khaleefi, A. L., & Al-Sanee, A. (2016). An experimental investigation of shear-transfer strength of normal and high strength self compacting concrete. *Engineering Structures*, 109, 16-25.

Rahal, K. N., Hassan, W. (2021). Shear strength of plain concrete made of recycled low-strength concrete aggregates and natural aggregates. *Construction and Building Materials*, 311, 125317.

Revilla-Cuesta, V., Faleschini, F., Pellegrino, C., Skaf, M., & Ortega-López, V. (2022). Simultaneous addition of slag binder, recycled concrete aggregate and sustainable powders to self-compacting concrete: a synergistic mechanical-property approach. J*ournal of Materials Research and Technology*, 18, 1886-1908.

Roslan, N. H., Ismail, M., Khalid, N. H. A., & Muhammad, B. (2020). Properties of concrete containing electric arc furnace steel slag and steel sludge. *Journal of Building Engineering*, 28, 101060.

Ruiz, M. F., Muttoni, A., & Sagaseta, J. (2015). Shear strength of concrete members without transverse reinforcement: A mechanical approach to consistently account for size and strain effects. *Engineering Structures*, 99, 360-372.

Ruiz, M. F. (2021). The influence of the kinematics of rough surface engagement on the transfer of forces in cracked concrete. *Engineering Structures*, 231, 111650.

Sagaseta, J., & Vollum, R. L. (2011). Influence of aggregate fracture on shear transfer through cracks in reinforced concrete. *Magazine of Concrete Research*, 63(2), 119-137.

Santamaría, A., Orbe, A., Losañez, M. M., Skaf, M., Ortega-Lopez, V., & González, J. J. (2017). Self-compacting concrete incorporating electric arc-furnace steelmaking slag as aggregate. *Materials & Design*, 115, 179-193.

Santamaría, A., Ortega-López, V., Skaf, M., Chica, J. A., & Manso, J. M. (2020). The study of properties and behavior of self-compacting concrete containing Electric Arc Furnace Slag (EAFS) as aggregate. *Ain Shams Engineering Journal*, 11(1), 231-243.

Santamaría, A., Romera, J. M., Marcos, I., Revilla-Cuesta, V., & Ortega-López, V. (2021). Shear strength assessment of reinforced concrete components containing EAF steel slag aggregates. *Journal of Building Engineering*, 103730.

Silva, R. V., de Brito, J. & Dhir, R. K. (2015). Tensile strength behaviour of recycled aggregate concrete. *Construction and Building Materials*, 83, 108-118.

Soetens, T., & Matthys, S. (2017). Shear-stress transfer across a crack in steel fibre-reinforced concrete. *Cement and Concrete Composites*, 82, 1-13.

Sun, C., Xiao, J., & Lange, D. A. (2018). Simulation study on the shear transfer behavior of recycled aggregate concrete. *Structural Concrete*, 19(1), 255-268.

Tamayo, P., Pacheco, J., Thomas, C., de Brito, J. & Rico, J. (2019). Mechanical and durability properties of concrete with coarse recycled aggregate produced with electric arc furnace sag concrete. *Applied Sciences*, 10(1), 216.

Trindade, J., Garcia, S., & Fonseca, G. (2020). Experimental Study of Direct Shear in Concrete with Recycled Aggregate. *ACI Structural Journal*, 117(5), 233-243.

UNI EN 197-1. (2011). Cement - Part 1: Composition, specifications and conformity criteria for common cements.

UNI EN 206-1. (2014). Concrete - Specification, performance, production and conformity.

Waseem, S. A., & Singh, B. (2016). Shear transfer strength of normal and high-strength recycled aggregate concrete–An experimental investigation. *Construction and Building Materials*, 125, 29-40.

Walraven, J. C. (1981). Fundamental analysis of aggregate interlock. *Journal of the Structural Division, ASCE*, 107(11), 2245-2270.

Xiao, J., Xie, H., & Yang, Z. (2012). Shear transfer across a crack in recycled aggregate concrete. *Cement and Concrete Research*, 42(5), 700-709.

Yang, Y., Walraven, J., & Uijl, J. D. (2017). Shear behavior of reinforced concrete beams without transverse reinforcement based on critical shear displacement. *Journal of Structural Engineering*, 143(1), 04016146.

Yusuf, M., St-Onge, P., Sarhat, S., & Green, M. (2019). Shear Transfer Strength of Concrete made with Recycled Concrete Aggregate after Exposure to High Temperatures. In *Third International Fire Safety Symposium*, Ottawa, Ontario, Canada (pp. 305-314).

Zanini, M. A. (2019). Structural reliability of bridges realized with reinforced concretes containing electric arc furnace slag aggregates. *Engineering Structures*, 188, 305-319.

Table 1. Aggregates physical properties.

	NA 0-4 mm	NA 4-16mm	EAF 4-8mm	EAF 8-12mm	EAF 8-16mm
Density s.s.d. (kg/m^3)	2644	2769	3840	3800	3784
Water absorption 24 h (%)	2.71	1.37	0.89	1.01	0.82
Shape	round	round	sharp	sharp	sharp

Table 2. Concrete mix design (kg for 1 m^3).

	NAC	EAF
Cement IV/A (V) 42.5 R	400	400
Water	200	200
w/c	0.5	0.5
NA 0-4 mm	862.5	862.5
NA 4-16 mm	1026.5	-
EAF 4-8 mm	-	501.9
EAF 8-12 mm	-	358.6
EAF 8-16 mm	-	563.0
SP	3.2	4.8

Table 3. Steel bar properties (average of three samples per each bar diameter d_s).

	d_s = 10 mm	d_s = 6 mm
f_y (MPa)	545.8	515.7
f_t (MPa)	679.8	602.1
ε_y (%)	0.32	0.31
ε_t (%)	9.67	9.79

Accepted manuscript doi:
10.1680/jmacr.22.00280

Table 4. Fresh and hardened concrete properties.

	NAC	EAF
ρ_c (kg/m^3)	2407	2824
Slump (cm)	12.0	10.0
$\rho_{c,28}$ (kg/m^3)	2431	2828
14d f_c (MPa)	32.48	46.98
28d f_c (MPa)	38.96	53.34
56d f_c (MPa)	43.89	58.81
28d f_{ct} (MPa)	3.56	4.56
28d E_c (GPa)	28.142	38.289

Table 5. Experimental vs. predicted mechanical concrete properties.

	f_{ctm} *exp.* (MPa)	f_{ctm} ACI318 (MPa)	f_{ctm} EC2 (MPa)	E_{cm} (GPa)	E_{cm} ACI318 (GPa)	E_{cm} EC2 (GPa)
NAC	3.56	3.50	2.96	28.142	29.336	33.083
EAF	4.56	4.09	3.81	38.289	34.326	36.356 (38.170*)

* applying a density-correction factor for EAF aggregates

Table 6. Push-off test: main results.

	P_u (kN)	τ_u (MPa)	s_u (mm)	w_u (mm)
NAC_1	54.98	6.11	0.511	0.054
NAC_2	46.44	5.16	0.303	0.025
NAC_3	57.00	6.33	0.466	0.037
ave.	*52.81*	*5.86*	*0.427*	0.039
st.dev.	*5.61*	*0.62*	*0.109*	0.015
EAF_1	70.37	7.82	0.316	0.026
EAF_2	60.98	6.78	0.248	-
EAF_3	73.80	8.20	0.393	0.050
ave.	*68.38*	*7.60*	*0.319*	0.038
st.dev.	6.64	*0.74*	*0.073*	0.017

Table 7. Dimensionless shear strength.

	τ_u^* (-)	τ_u^+ (-)
NAC_1	0.98	1.72
NAC_2	0.83	1.45
NAC_3	1.01	1.78
ave.	*0.94*	*1.65*
st.dev.	*0.10*	*0.17*
EAF_1	1.07	1.71
EAF_2	0.93	1.49
EAF_3	1.23	1.80
ave.	*1.04*	*1.67*
st.dev.	*0.10*	*0.16*

Table 8. Predicted shear strength from Coulomb failure criterion – based formulations.

Reference	$\tau_u = c$	$\tau_{u,th}\,NAC$ (MPa)	Δ_{NAC} (-)	$\tau_{u,th}\,EAF$ (MPa)	Δ_{EAF} (-)
Sagaseta and Vollum (2011) gravel	$c = 0.57 \cdot f_{ctk}$	2.029	0.346	2.599	0.342
Sagaseta and Vollum (2011) limestone	$c = 0.91 \cdot f_{ctk}$	3.239	0.552	4.150	0.546
ACI318 monolithic ordinary (2019)	c = 2.75 MPa	2.750	0.469	2.750	0.362
ACI318 rough ordinary (2019)	c = 2.75 MPa	2.750	0.469	2.750	0.362
ACI318 medium ordinary (2019)	-	-	-	-	-
EC2 rough surface (2004)	$c = 0.4 \cdot f_{ctd}$	1.424	0.243	1.824	0.240
EC2 smooth (2004)	$c = 0.2 \cdot f_{ctd}$	0.712	0.121	0.912	0.120
EC2 very smooth (2004)	$c = 0.025\text{-}0.1 \cdot f_{ctd}$	0.356	0.061	0.456	0.060
Hamadi and Regan gravel (1980)	c = 4 MPa	4.000	0.682	4.000	0.526
Hamadi and Regan expanded clay (1980)	c = 2 MPa	2.000	0.341	2.000	0.263
Climaco and Regan rough (2001)	$c = 0.25 \cdot f_c^{2/3}$	2.873	0.490	3.542	0.466
Climaco and Regan medium (2001)	$c = 0.25 \cdot f_c^{2/3}$	2.873	0.490	3.542	0.466
Climaco and Regan smooth (2001)	c = 0.5 MPa	0.500	0.085	0.500	0.066

Figure captions

Figure 1. a) push-off specimen; b) FIP specimen; c) Modified JSCE SF6 specimen.
Figure 2. Electric Arc Furnace slag with different particles size.
Figure 3. Aggregates grading curve.
Figure 4. Push-off specimens: geometry and reinforcement details (measures in mm).
Figure 5. Push-off test setup and instrumentation disposition.
Figure 6. Failure mode and cracks in front and back faces of: a) NAC_2; b) EAF_1 specimens.
Figure 7. Crack paths in the shear planes: a) NAC_2; b) EAF_1 specimens.
Figure 8. Shear cracks in plain concrete: a) cracks around the aggregate; b) cracks through the aggregate.
Figure 9. Shear stress vs. slip curves.
Figure 10. Shear stress vs. crack opening curves.
Figure 11. Comparison of dimensionless shear strength among NAC, RAC and EAF concretes.

Accepted manuscript doi:
10.1680/jmacr.22.00280

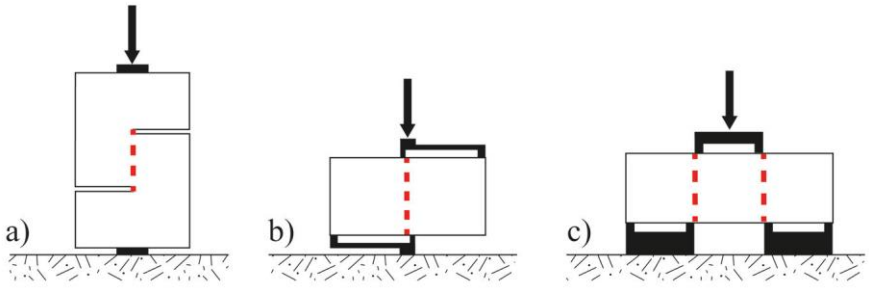

Figure1

Stampa

Accepted manuscript doi:
10.1680/jmacr.22.00280

HERE FIGURE 2 SHOULD BE PLACED.

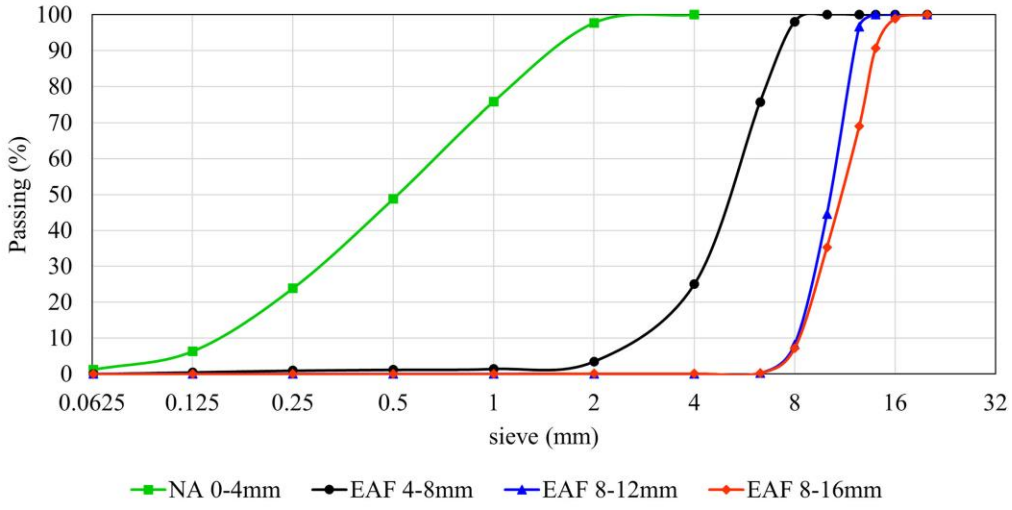

Figure2

FIGURE 3

Accepted manuscript doi:
10.1680/jmacr.22.00280

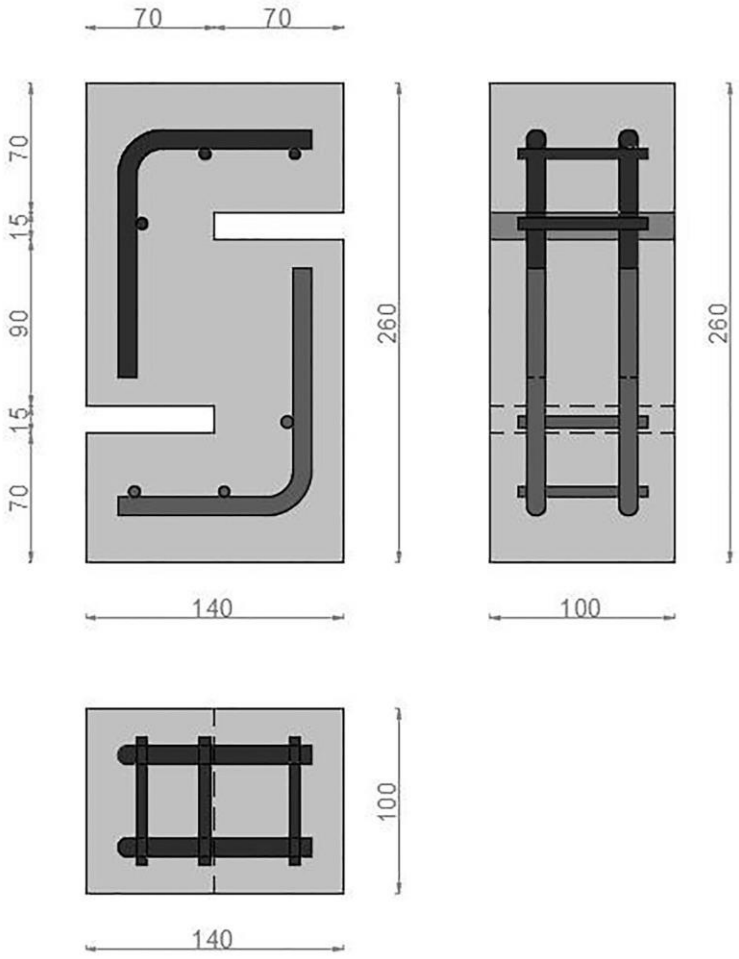

Figure3

FIGURE 4

Accepted manuscript doi:
10.1680/jmacr.22.00280

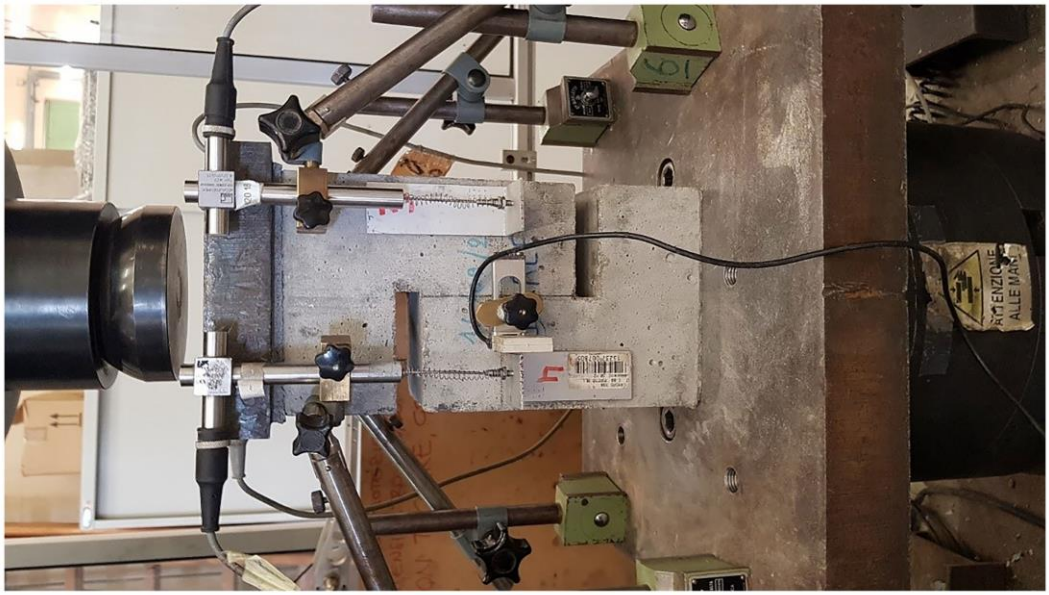

Figure4

FIGURE 5

Accepted manuscript doi:
10.1680/jmacr.22.00280

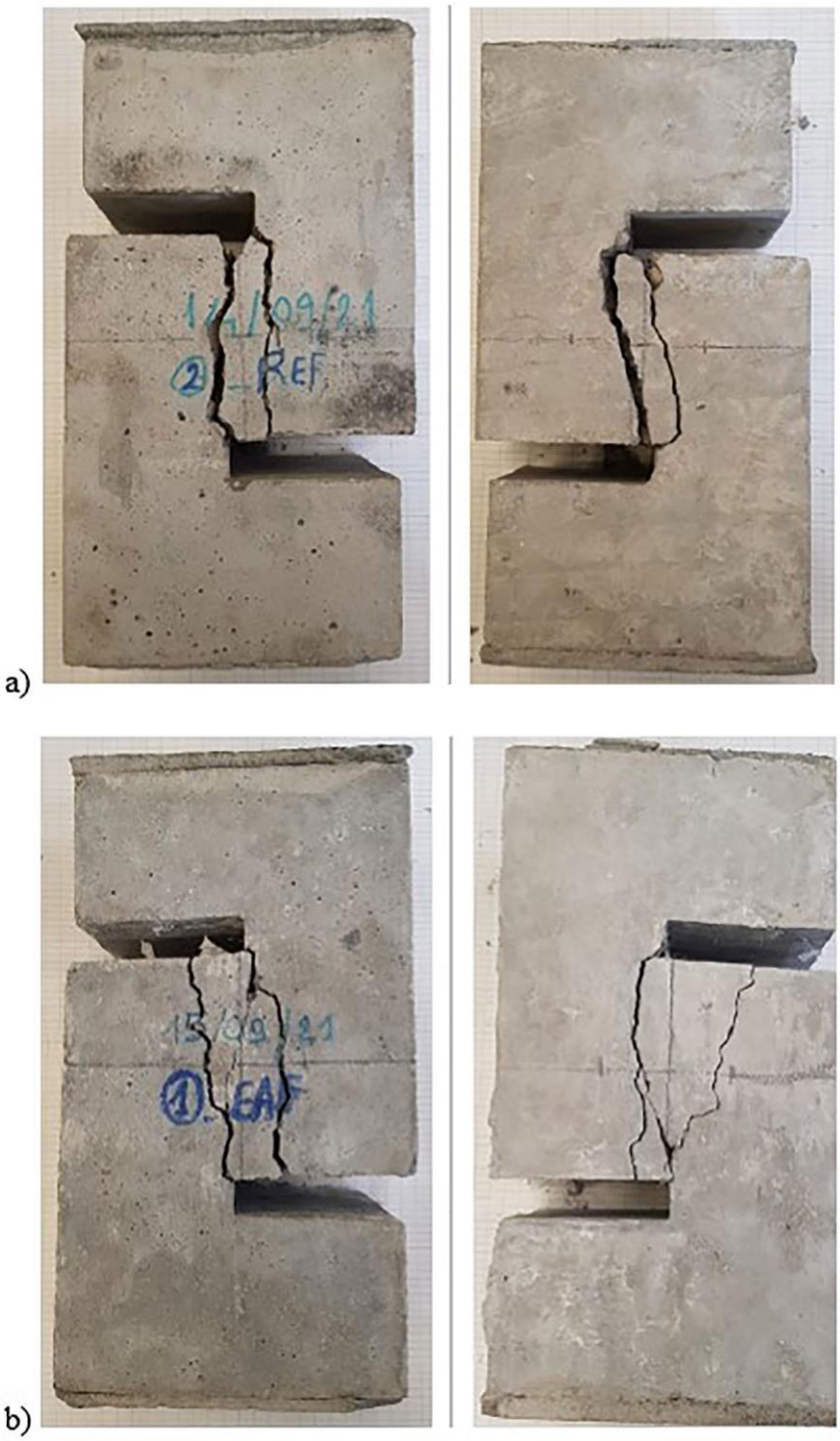

Figure 6

Accepted manuscript doi:
10.1680/jmacr.22.00280

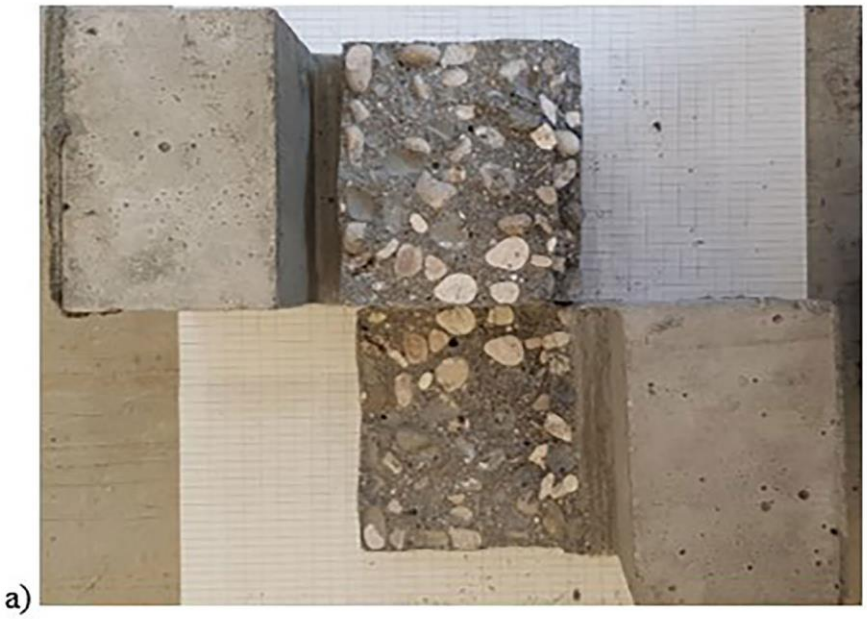

a)

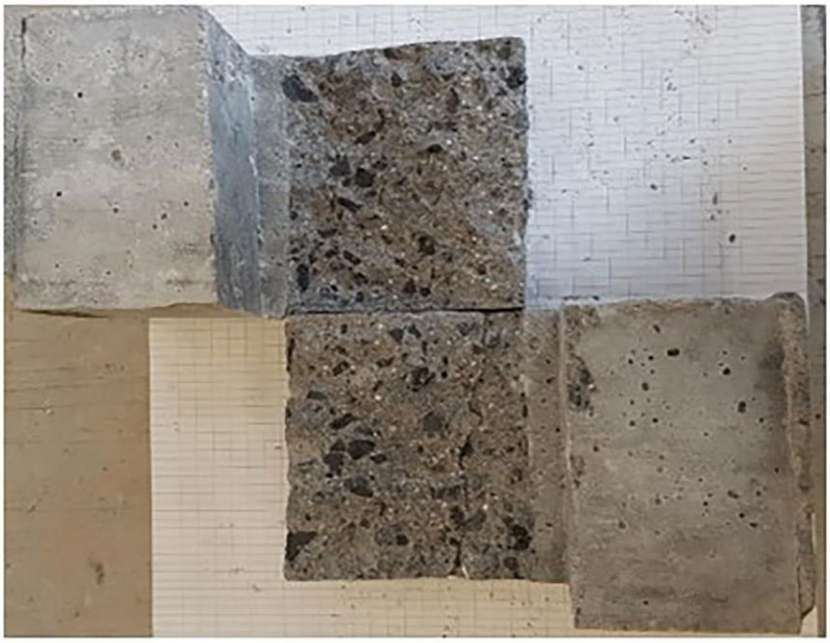

b)

Figure 6

FIGURE 7

Accepted manuscript doi:
10.1680/jmacr.22.00280

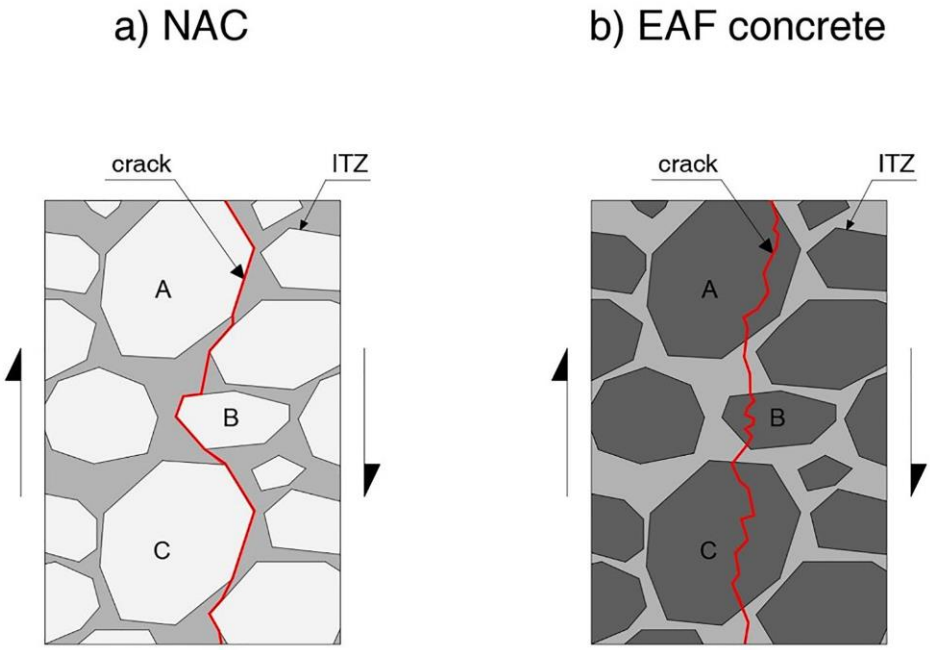

Figure 7

FIGURE 8

Accepted manuscript doi:
10.1680/jmacr.22.00280

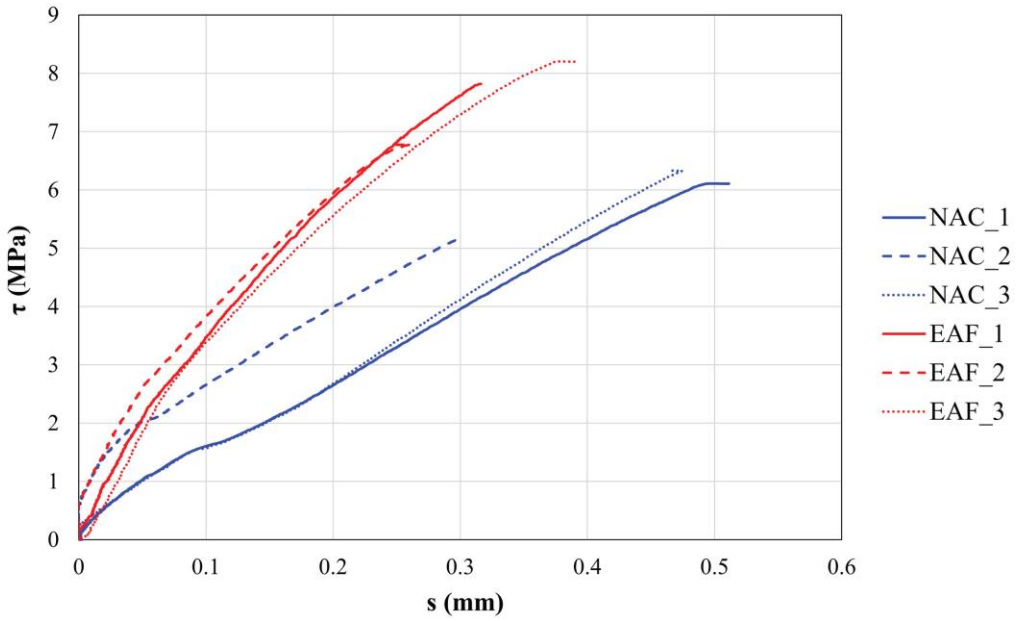

Figure8

FIGURE 9

Accepted manuscript doi:
10.1680/jmacr.22.00280

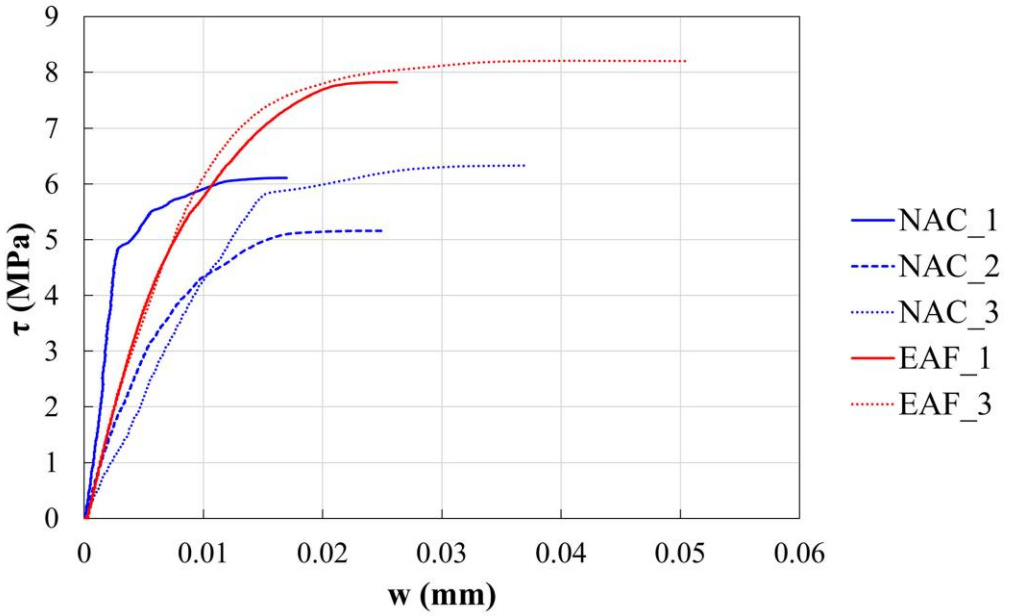

Figure 10

FIGURE 10

Accepted manuscript doi:
10.1680/jmacr.22.00280

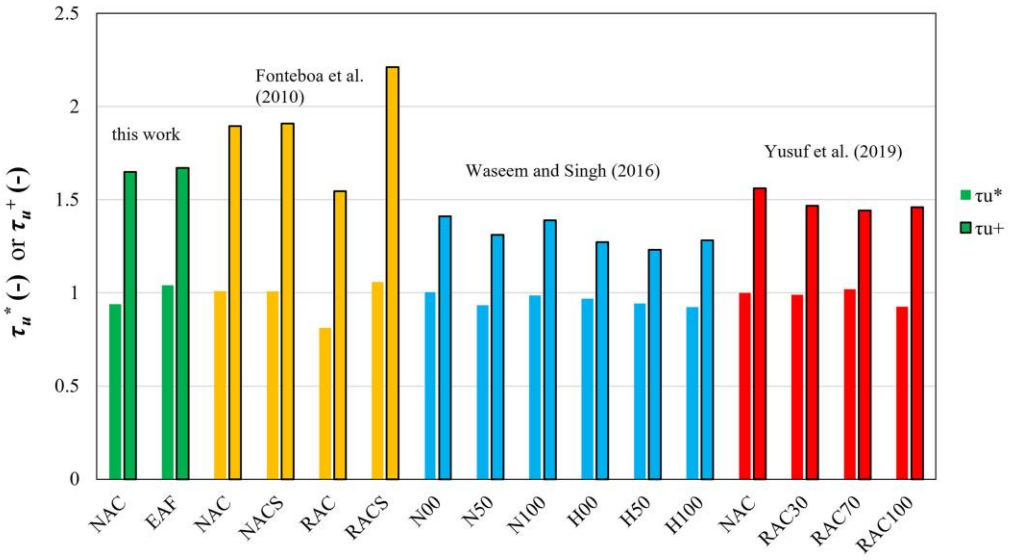

Figure 11

FIGURE 11

Accepted manuscript doi:
10.1680/jmacr.22.00280

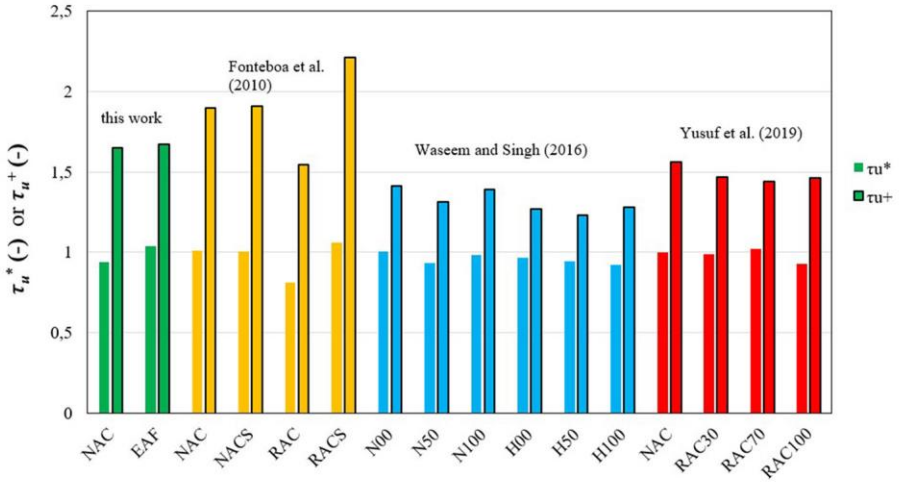

Figure11